Electronic Supplementary Information

Aerobic oxidation of alcohols using a slurry loop membrane reactor

Baldassarre Venezia and Asterios Gavriilidis*

Dept of Chemical Engineering, University College London, Torrington Place, London WC1E 7JE, UK

Contents

Reactor component design and experimental setup 2
Saturator 2
Crossflow filter 5
Heating units 7
Experimental setup 7
Macromixing study 8
Styrene hydrogenation and gas-liquid mass transfer 10
Catalyst particle size distribution 10
k_La determination 10
Styrene hydrogenation 13
Specific power input 16
Aerobic oxidation of alcohols 17
Catalyst particle size distribution 17
Temperature distribution in the loop 18
Continuous operation 19
Benzyl alcohol 19
Cinnamyl alcohol 24
Geraniol 26
1-Phenylethanol 27
Piperonyl alcohol 28
Pervaporation rate and safety considerations 31
References 33

*Corresponding author's email address: a.gavriilidis@ucl.ac.uk

Reactor component design and experimental setup

Saturator

The saturator was made of two parts in stainless steel (316L), one hosting the serpentine channel for the slurry flow and a second one designed for delivering the gaseous reactants. Between the two, a Teflon AF-2400 membrane (0.023'' thickness, Biogeneral US) was sandwiched and was in direct contact with the slurry flow. Figure S1 shows the saturator part with the serpentine channel for the slurry. There were three lateral holes for three cartridge heaters. The slurry mixture entered and exited the saturator via two holes (1/4-28 UNF) at 30° to prevent clogging of the channel by the catalyst particles in the slurry. Two further holes on both ends of the serpentine channel were designed to allow for pressure measurements, one of which was also used to introduce the neat liquid substrate in the loop. The serpentine channel was 0.30 mm deep, 6 mm wide and each straight section of the channel was separated by 7.7 mm distance from each other. The channel had 5 U-turns, a length of 808 mm and a surface area of 4850 mm^2.

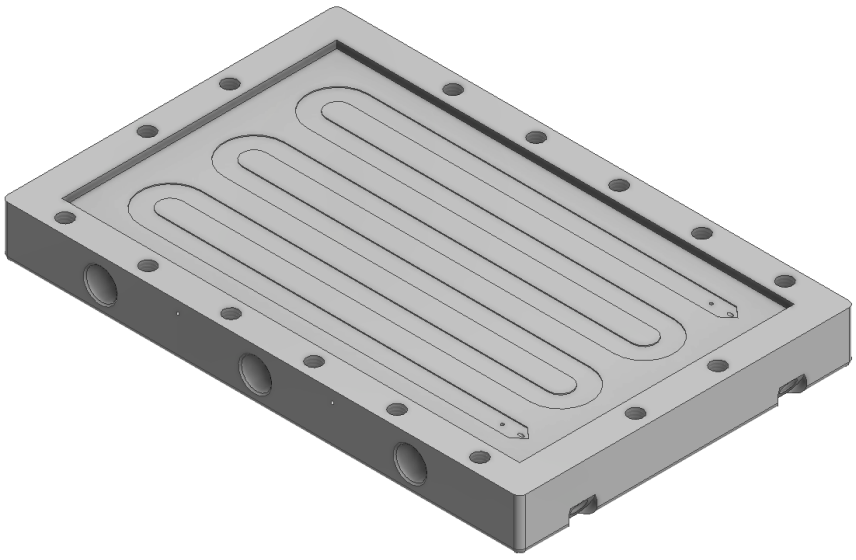

Figure S1. Top part of the saturator hosting the channel for the slurry flow.

The Teflon AF-2400 membrane was placed over an area of 90 mm x 150 mm at the centre of the block, covering the whole serpentine channel.

The part of the saturator hosting the gas channel is featured in Figure S2. The channel was surrounded by a 2 mm thick edge and in between each straight section a series of fins of 1 mm x 124 mm were designed. Both the edge and the fins were 0.50 mm higher compared to the channel surface and were devised in order to exert pressure on the gasket around the slurry channel in order to prevent internal bypasses. The 2 mm thick edge was designed to enclose the whole serpentine in order to hinder external leakage. The gas inlet and outlet ports were perpendicular to the serpentine gas channel.

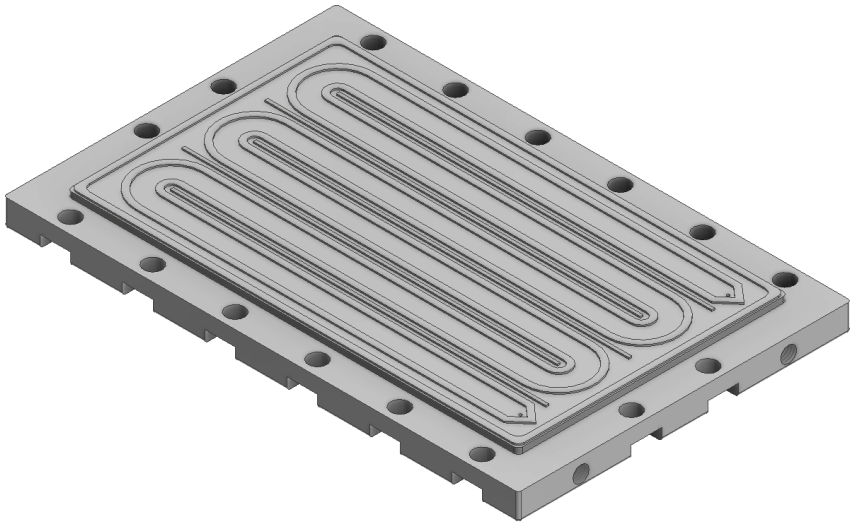

Figure S2. Bottom part of the saturator hosting the gas channel.

The saturator assembly is presented in Figure S3. On the left-hand side it is possible to see the individual parts inside the saturator. Above the Teflon AF-2400 membrane, a 304 stainless steel mesh (Industrial Netting) was placed to provide mechanical stability to the membrane. The mesh had the same length (150 mm) and width (90 mm) as the membrane, but with a thickness of 0.05 mm. Furthermore, it was covered by microholes for 23% of the total area, each with an average diameter of 76 μm. In order to create a seal between the mesh and the gas channel, a Kalrez® gasket (DuPont) with a thickness of 0.5 mm was used. The gasket was cut and shaped to match the same geometry of the slurry channel and placed on top of the metal mesh. The saturator was then tightened with sixteen M6x50 bolts (ISO 4762), flipped over and further tightened with two clamps held together by four M8x60 bolts (ISO 4762).

The clamps had a set of ten pillars on each side that exerted pressure on the center of the saturator and avoided internal bypasses within the slurry channel. In Figure S3 (right) it is possible to see two holes (1/4-28 UNF) on the top part of the saturator, which were used to measure the slurry pressure across the serpentine. The hole on the left was also used as inlet port for introducing the reaction substrates during continuous operation.

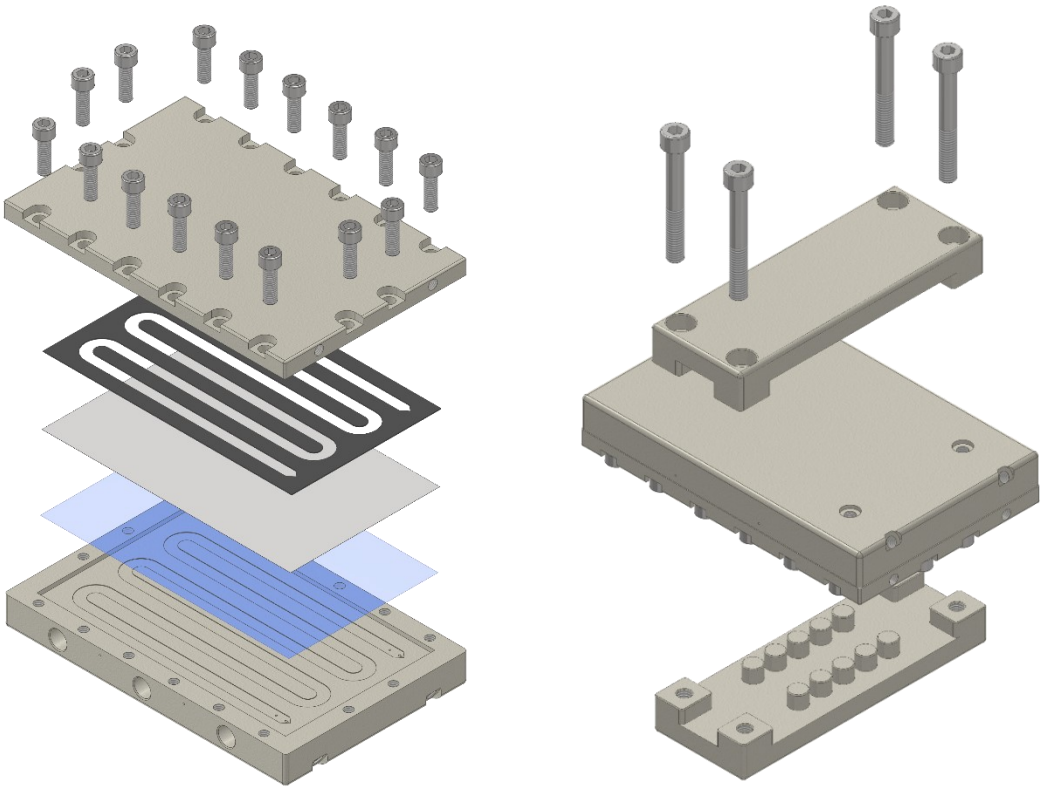

Figure S3. Exploded assemblies of the saturator. On the left: The Teflon AF-2400 membrane (blue), the metal mesh (light grey) and the gasket (black) were assembled inside the saturator. On the right: The saturator is shown upside down before being tightened with two clamps.

Pictures of the saturator are shown in Figure S4. Holes for the thermocouples were distributed around the saturator, while the cartridge heaters were inserted from one side and the wires collected outside the Delrin® acetal box.

Figure S4. Pictures of the saturator showing where thermocouples and cartridge heaters were inserted.

Crossflow filter

The filter unit was made of two blocks of stainless steel 316L, a top and a bottom part. The former hosted the slurry channel and was connected to the loop, while the bottom part collected the filtered liquid from the slurry and was connected to the outlet of the reactor. Figure S5 shows the cassette-type assembly of the crossflow filter. A sintered stainless steel filter (0.1 µm 316L, Mott) was placed between the two blocks and was sealed using a Kalrez® O-ring (cross section diameter: 2.62 mm, DuPont) and a Kalrez® gasket (thickness: 0.50 mm, DuPont). Fourteen M2.5x20 bolts (ISO 4762) ensured that the filter was tightened enough to withstand the operating pressure of the slurry in the loop. A characteristic feature of the filter top part was the 30° angle at which the inlet and the outlet ports were connected to the loop with respect to the sintered filter, and this was done to hinder catalyst clogging in the channel. The slurry channel in the filter was 0.5 mm deep, 2 mm wide and 25 mm long, and an average

slurry velocity of 16.7 cm/s was achieved in the slurry channel, when a 10 mL/min recycle flowrate through the filter was used.

An O-ring was fitted in the groove of the bottom part, while the gasket and the stainless steel filter were placed on the area surrounded by the groove. A hole of 1 mm diameter was drilled to connect the channel for the collection of filtered liquid to the hole (1/4-28 UNF) of the outlet.

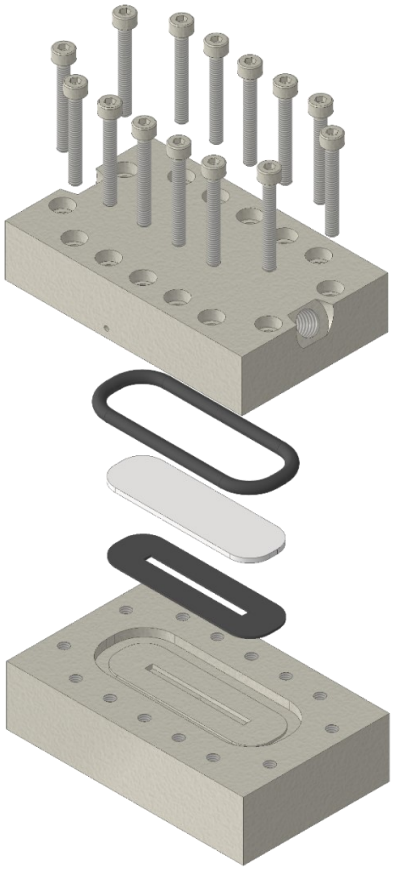

Figure S5. Exploded assembly of the crossflow filter used in the slurry loop membrane reactor.

Heating units

In order for the reactor to operate up to 120 °C, the saturator had three cartridge heaters (10 mm x 70 mm, 250 W, RS Components) inserted, and covered by thermal grease (10 W/m/K, RS Components). Furthermore, a silicon heater mat (100 mm x 150 mm, 15 W, RS Components) was placed below the crossflow filter and the pump head, and a polyimide flexible heater (10 W/in^2, Omega) was attached to the crossflow filter. Seven holes for thermocouples (T type, RS Components) were drilled around the saturator and one hole in the filter at 1 - 2 mm below the slurry channel, in order to measure the temperature profile and allow for heating control. The process thermocouple was inserted in the saturator (see the section “Temperature distribution in the loop”) and connected to a temperature control box, which controlled the power of the heaters to achieve the desired temperature setpoint.

Experimental setup

Figure S6 shows a picture of the setup with the reactor inside a case made of Delrin® acetal on the lowest level. The piston pump for the substrate delivery was placed in the middle shelf and the gas flowrate control box on the top shelf. The temperature control boxes can be seen on the left and the vessels containing the alcohol substrate and those collecting the liquid products on the right hand side.

Figure S6. Picture of the slurry loop membrane reactor setup.

Macromixing study

Macromixing was evaluated by studying the residence time distribution (RTD) of the slurry loop membrane reactor. Experiments were conducted using DI water at atmospheric pressure and room temperature (21 °C). The schematic of the setup is shown in Figure S7. A syringe pump (Harvard Apparatus PHD 2000) was used to pump DI water from a syringe (50 mL, SHE). Connected to the syringe was a perfluoro alkoxy capillary tube (PFA, 1/16'' OD x 0.040'' ID, Idex) filled with 100 µL of 7.5 g/L of blue tracer (Basic Blue 3, Sigma Aldrich) and connected at the outlet and the inlet by two shut-off valves (0.04'' ID hole, Kinesis). Before injecting the tracer, all the tubings were filled with DI water, including the loop. The recirculation flowrate was set to 10 mL/min and the valves at both the two ends of the tracer-filled tubing were opened and the syringe pump was switched on. Macromixing was studied at different inlet flowrates ranging from 0.1 mL/min to 1 mL/min and the elapsed time was taken from the moment the tracer entered the loop.

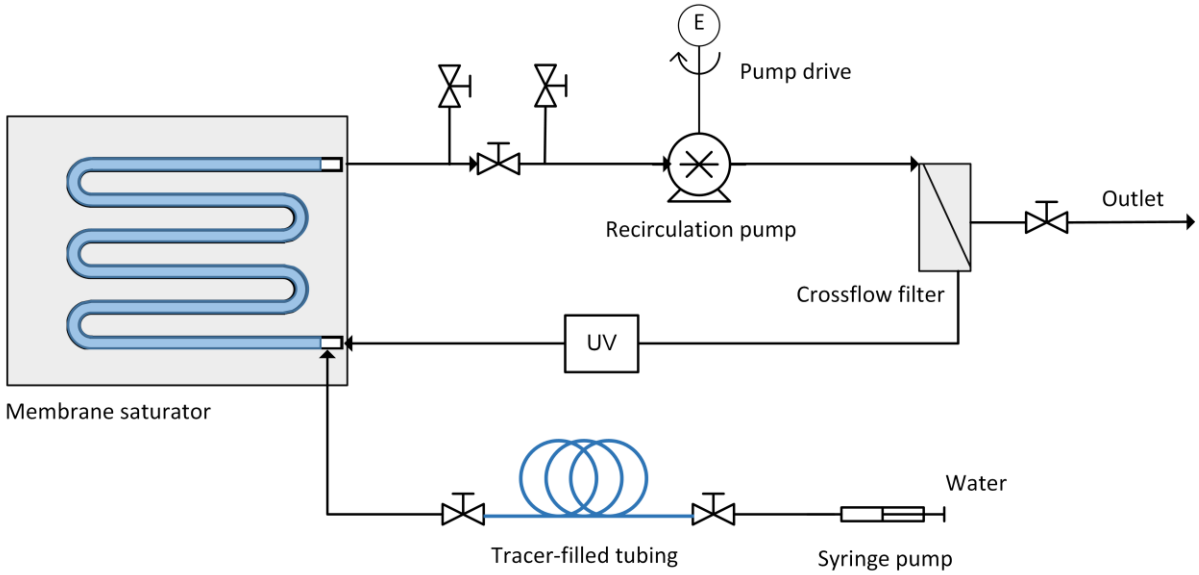

Figure S7. Setup schematic of the slurry loop membrane reactor for the macromixing study. The tracer was introduced by a pulse-input injection. The flow cell of the UV-vis spectrophotometer (UV) was installed directly in the loop.

The UV-Vis flowcell (UV) was directly installed in the loop. The transmitted light was detected by a spectrophotometer (Ocean Optics USB2000+ UV-VIS-ES) and subtracted as background (only DI water) before the experiment. During the analysis, the integration time was set to 4 ms and the intensity of the transmitted light was

averaged between 645 and 660 nm, which corresponds to the wavelength range of the blue dye peak intensity. Data analysis was performed using the software Ocean Optics Spectra Suite. The concentration of the tracer can be related to the absorbance according to the Beer-Lambert law, shown in Equation (S1), where *A* stands for the absorbance, *I* and I_o the transmitted and the incident light intensity, respectively, φ the extinction coefficient, *L* the absorption length and *C* the tracer concentration. Calibration of the spectrophotometer was performed to make sure that the tracer concentration in the loop lied within the range where absorbance and tracer concentration are linearly proportional.

$$A = -\log\left(\frac{I}{I_0}\right) = \varphi L C \tag{S1}$$

Given the proportionality between the absorbance and the concentration, the residence time distribution, *E(t)*, was derived, as shown in Equation (S2). The average residence time, τ, was determined by integrating the first moment of *E(t)*, see Equation (S3). Finally, the dimensionless residence time distribution, *E(θ),* and time, *θ*, were derived to compare the RTDs at different recycle ratios, using Equation (S4).

$$E(t) = \frac{C(t)}{\int_0^\infty C(t)\,dt} = \frac{A(t)}{\int_0^\infty A(t)\,dt} \tag{S2}$$

$$\tau = \int_0^\infty t\,E(t)dt \tag{S3}$$

$$E(\theta) = \tau\,E(t); \quad \theta = {}^{t}/_{\tau} \tag{S4}$$

The resulting data from the macromixing study were compared to the residence time distribution of a CSTR, $E_{CSTR}(\theta)$ (see Equation (S5)). The discrepancy between the two was calculated using the normalised residual sum of squares (*RSS*). Equation (S6) shows the *RSS*, where *N* is the total number of experimental points.

$$E_{CSTR}(\theta) = e^{-\theta} \tag{S5}$$

$$RSS = \frac{1}{N}\sum_i^N [E(\theta_i) - E_{CSTR}(\theta_i)]^2 \tag{S6}$$

Styrene hydrogenation and gas-liquid mass transfer

Catalyst particle size distribution

The particle size distribution of the 5 wt% Pd/C catalyst (type 487, Alfa Aesar) was determined via laser diffraction (LS 13 320, Beckman Coulter) and the result is shown in Figure S8.

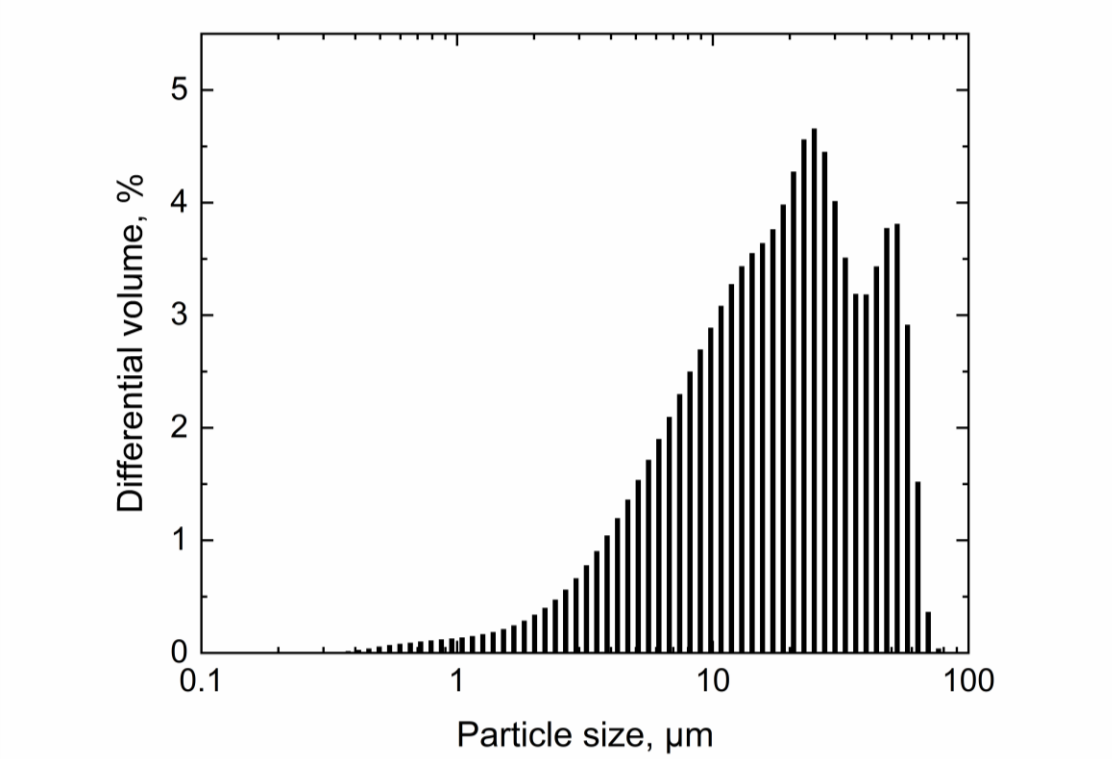

Figure S8. Particle size distribution of the 5 wt% Pd/C employed in the gas-liquid mass transfer study in the slurry loop membrane reactor

k_La determination

Equation (1) in the manuscript is derived considering all the steps in the transport of hydrogen from the bulk gaseous phase to the catalyst particles in the slurry where it reacted with styrene. In this derivation it is assumed that the mass transport of styrene is not limited by resistances, due to its relatively high concentration (2 M). The absorption of hydrogen in the gas phase onto the membrane is governed by Equation (S7), where r_{H2} is the volumetric rate of transport, k_G the hydrogen mass transfer coefficient in the gas phase, a the surface membrane area-to-reactor volume ratio, $p_{H2,bG}$ the pressure of hydrogen in the bulk gas phase, $p_{H2,iG}$ the pressure of hydrogen on the surface of the membrane and H_E the Henry constant of hydrogen.

$$r_{H_2} = k_G a \left(\frac{p_{H_2,bG}}{H_E} - \frac{p_{H_2,iG}}{H_E} \right) \quad \text{(S7)}$$

However, for slightly soluble gases or pure gases, like in this work, the adsorption and dissolution of hydrogen onto the membrane can be neglected [1]. Therefore, $p_{H2,bG}$ and $p_{H2,iG}$ can be considered as equal to each other (4 bar).

The mass transport of hydrogen across the Teflon-AF 2400 membrane can be written as in Equation (S8). Here, $k_{H2,m}$ is the hydrogen permeability across the membrane, $C_{H2,i}$ the hydrogen concentration on the membrane-liquid interface and d_m the membrane thickness.

$$r_{H_2} = \frac{k_{H_2,m}\, a \left(p_{H_2,iG} - C_{H_2,i}\, H_E \right)}{d_m} \quad \text{(S8)}$$

Assuming the concentration of hydrogen at the membrane-liquid interface equal to zero, the maximum molar flow of hydrogen that can be delivered by the membrane would be $3.8 \cdot 10^{-6}$ mol/s, which translates into 0.114 mL/min of 2 M styrene in methanol being fully converted to ethylbenzene. Table S1 shows the membrane properties from which the hydrogen molar flow can be calculated using Equation (S8), where $p_{H2,iG}$ is equal to 4 bar.

Table S1.

Properties of the Teflon AF-2400 membrane used in this work.

Property	Value
Hydrogen permeability [2], barrer	3600
Membrane thickness, mm	0.58
Surface area, mm^2	4850
Specific surface area, m^{-1}	3460

Experiments performed at 0.050 mL/min did not show full conversion (*vide infra*), suggesting that the rate limiting step was not the hydrogen transport across the membrane.

It is now possible to set Equation (S8) equal to zero and determine $C_{H2,i}$ as a ratio between $p_{H2,iG}$ and H_E. Under the temperature (21 °C) and pressure (4 bar) employed in this work, the Henry constant for the hydrogen-methanol system was calculated

according to Equation (S9) and a value of 674 MPa/M was determined [1]. The concentration of hydrogen at the interface of the membrane with the liquid, $C_{H2,i}$, at 4 bar was estimated to be equal to $5.93 \cdot 10^{-4}$ M.

$$\ln(H_E) = 122.3 - \frac{4815.6}{T} - 17.5\ln(T) + 1.4 \cdot 10^{-7} p_{H_2} \quad \text{(S9)}$$

Once diffused through the membrane, hydrogen must diffuse into the bulk liquid and on the catalyst surface where it reacts with styrene. The hydrogen transport in the liquid phase can be described using Equation (S10). Here, k_La stands for the volumetric gas-liquid mass transfer coefficient on the liquid side and $C_{H2,bL}$ is the hydrogen concentration in the bulk liquid phase. Equation (S11) describes the hydrogen transport from the bulk liquid phase to the catalyst surface ($C_{H2,s}$), where k_s is the liquid-solid mass transfer coefficient, a_p the external surface area of the catalyst per unit mass and ρ_{cat} is the catalyst concentration (g/L).

$$r_{H_2} = k_L a\left(C_{H_2,i} - C_{H_2,bL}\right) \quad \text{(S10)}$$

$$r_{H_2} = k_s a_p \rho_{cat}(C_{H_2,bL} - C_{H_2,s}) \quad \text{(S11)}$$

The diffusion of hydrogen through the pores of the catalyst particles and the reaction on the surface is summarised in Equation (S12), assuming first-order kinetics with respect to the concentration of hydrogen on the catalyst surface, $C_{H2,s}$. Here, η is the effectiveness factor and k' the pseudo-first order rate constant per unit of catalyst mass.

$$r_{H_2} = \eta \rho_{cat} k' C_{H_2,s} \quad \text{(S12)}$$

At steady-state, the abovementioned equations are equal to each other as shown in Equation (S13). Summing all the driving forces, it is possible to relate the concentration of hydrogen at the membrane-liquid surface, $C_{H2,i}$, to the individual mass transport resistances, as expressed in Equation (S14). This can be further rearranged into Equation (S15) which shows the overall mass transfer resistance as a function of the individual mass transfer resistances.

$$r_{H_2} = k_L a\left(C_{H_2,i} - C_{H_2,bL}\right) = k_s a_p \rho_{cat}(C_{H_2,bL} - C_{H_2,s}) = \eta \rho_{cat} k' C_{H_2,s} \quad \text{(S13)}$$

$$C_{H_2,i} = \frac{r_{H_2}}{k_L a} + \frac{r_{H_2}}{k_s a_p \rho_{cat}} + \frac{r_{H_2}}{\eta \rho_{cat} k'} \quad \text{(S14)}$$

$$\frac{C_{H_2,i}}{r_{H_2}} = \frac{1}{k_L a} + \frac{1}{\rho_{cat}}\left(\frac{1}{k_s a_p} + \frac{1}{\eta k'}\right) \quad \text{(S15)}$$

Styrene hydrogenation

At an inlet flowrate of 0.050 mL/min and a catalyst concentration of 0.60 g/L, the recycle flowrate, v_{rec}, was varied from 5 to 20 mL/min. Hydrogen pressure above the membrane and the reactor temperature were kept constant at 4 bar and 21 °C. Figure S9 shows the results. In spite of the fact that the reactor was operating under CSTR conditions (R > 100), conversion increased by increasing the recycle flowrate.

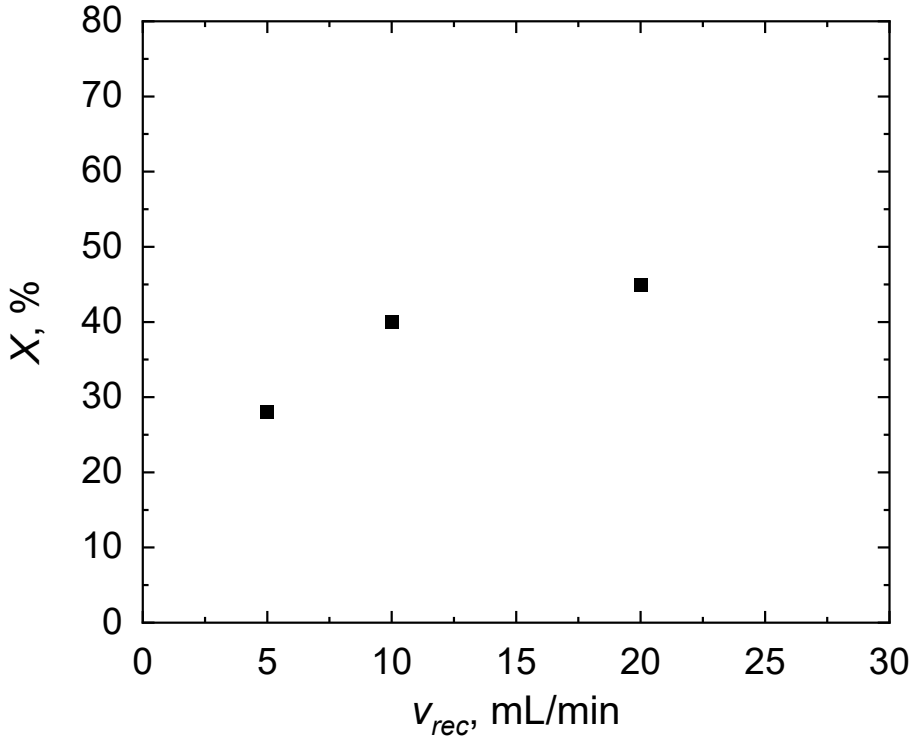

Figure S9. Styrene conversion, X, as a function of the recycle flowrate, v_{rec}, in the styrene hydrogenation to ethylbenzene using 5 wt% Pd/C powder catalyst. Styrene inlet concentration: 2 M, solvent: methanol, inlet flowrate: 0.050 mL/min, catalyst concentration: 0.60 g/L, hydrogen pressure: 4 bar, temperature: 21 °C, reactor volume: 1.4 cm^3, membrane specific surface area: 34.6 cm^{-1}.

However, only a 5% conversion increment was observed when increasing the flowrate from 10 mL/min to 20 mL/min. As discussed in the manuscript, above a catalyst concentration of 0.50 g/L styrene hydrogenation was limited by the gas-liquid mass

transfer resistance. Therefore, any increase in conversion can be ascribed to an enhancement of the gas-liquid mass transfer coefficient k_L.

The catalyst concentration was then varied in order to determine the k_La value. Experiments were performed at 10 mL/min at 4 bar and 21 °C. Figure S10 shows the experimental results, while the linear fitting of $C_{H2,i}/r_{H2}$ against $1/\rho_{cat}$ is presented in Figure S11.

Calculation of the volumetric reaction rate of hydrogen was done using Equation (S16). X is the styrene conversion, V_R is the reactor volume (1.4 mL) and v the inlet flowrate (0.050 mL/min).

$$r_{H_2} = \frac{v\ X\ C_{Sty,in}}{V_R} \tag{S16}$$

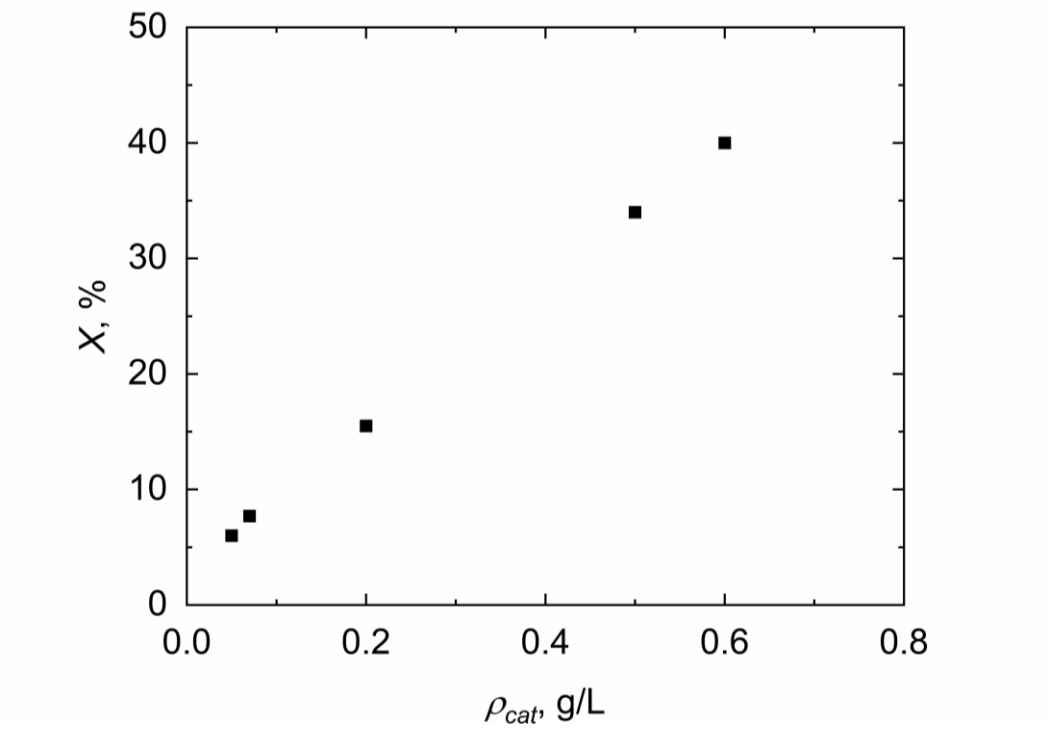

Figure S10. Styrene conversion, X, as a function of the catalyst concentration, ρ_{cat}, in the styrene hydrogenation to ethylbenzene using 5 wt% Pd/C powder catalyst. Styrene inlet concentration: 2 M, solvent: methanol, inlet flowrate: 0.050 mL/min, recycle flowrate: 10 mL/min, hydrogen pressure: 4 bar, temperature: 21 °C, reactor volume: 1.4 cm^3, membrane specific surface area: 34.6 cm^{-1}.

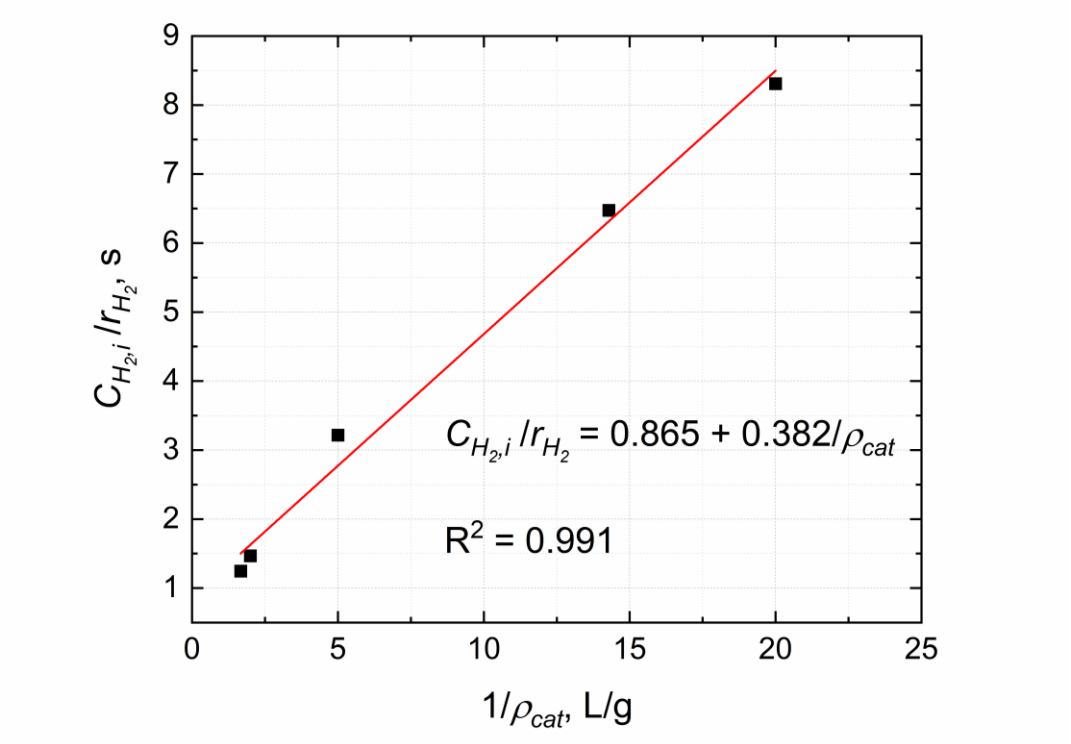

Figure S11. Hydrogen gas concentration at the membrane-liquid interface, $C_{H2,i}$, divided by the reaction rate, r_{H2}, against the inverse of the catalyst concentration, ρ_{cat}, for the styrene hydrogenation to ethylbenzene using 5 wt% Pd/C powder catalyst. Styrene inlet concentration: 2 M, solvent: methanol, inlet flowrate: 0.050 mL/min, recycle flowrate: 10 mL/min, hydrogen pressure: 4 bar, temperature: 21 °C, reactor volume: 1.4 cm^3, membrane specific surface area: 34.6 cm^{-1}.

Specific power input

The specific power input in the slurry loop membrane reactor can be derived from the Bernoulli equation. Equation (S17) shows the Bernoulli equation applied to the recirculation pump, in the case of equal kinetic and potential energy at the inlet and the outlet of the pump and no energy dissipation within the pump. p_1 and p_2 are the inlet and outlet pressures, respectively, while H_{pump} is the pump head. The pressure drop on the pump, Δp_{pump}, can be written as the power provided by the pump, P_{pump}, divided by the recycle flowrate of the slurry, v_{rec}, (Equation (S18)), and by definition, the power is the product of the volumetric power input, ε, and the reactor volume, V_R.

$$p_1 + H_{pump} = p_2 \tag{S17}$$

$$H_{pump} = p_2 - p_1 = \Delta p_{pump} = \frac{P_{pump}}{v_{rec}} = \frac{\varepsilon V_R}{v_{rec}} \tag{S18}$$

Aerobic oxidation of alcohols

Catalyst particle size distribution

The 1 wt% Au-Pd/TiO_2 catalyst (Johnson Matthey) employed in the aerobic oxidation of alcohols was characterised via laser diffraction (LS 13 320, Beckman Coulter) and the particle size distribution is shown in Figure S12.

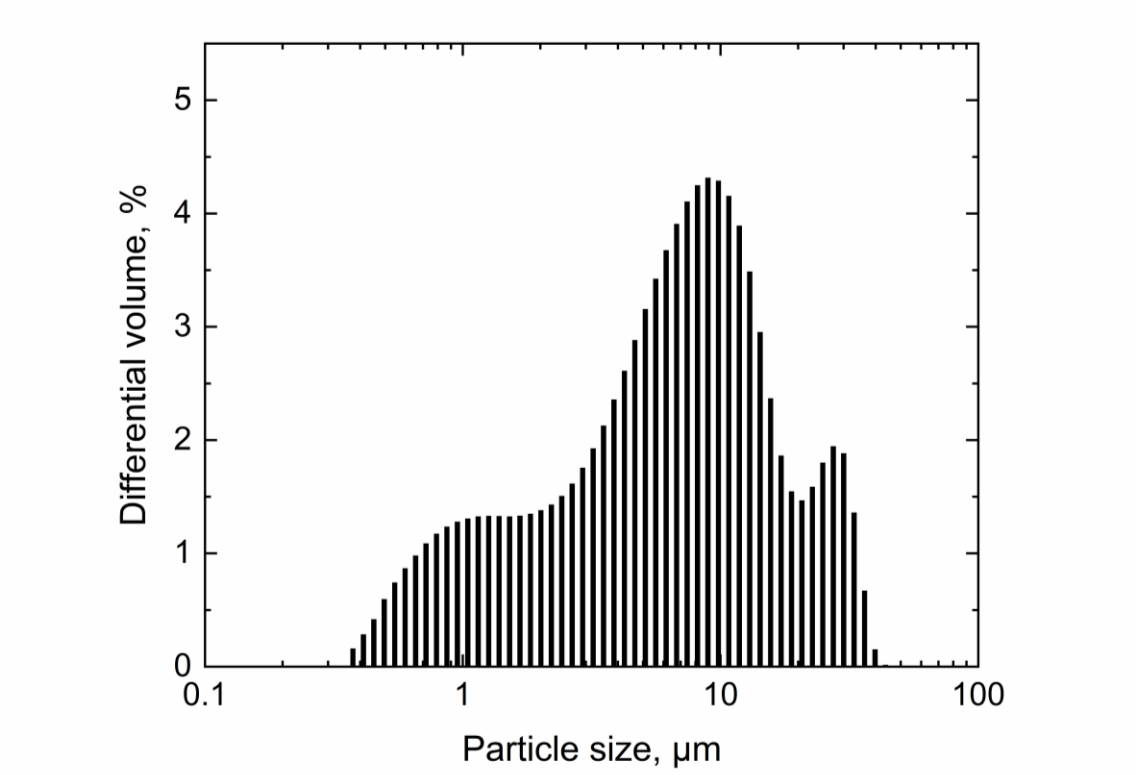

Figure S12. Particle size distribution of the 1 wt% Au-Pd/TiO_2 employed in the aerobic oxidation of alcohols using the slurry loop membrane reactor.

Temperature distribution in the loop

The loop reactor had eight different positions between the saturator and the crossflow filter where temperature could be monitored. Figure S13 shows the loop reactor inside the acetal box and the areas of temperature measurement. Table S2 reports temperature measurements during the solvent-free aerobic oxidation of benzyl alcohol at 6 bar oxygen pressure, 10 mL/min recycle flowrate and an overall temperature of 110 ± 1.4 °C. The process temperature thermocouple was inserted in position number 4, where the highest temperature was measured.

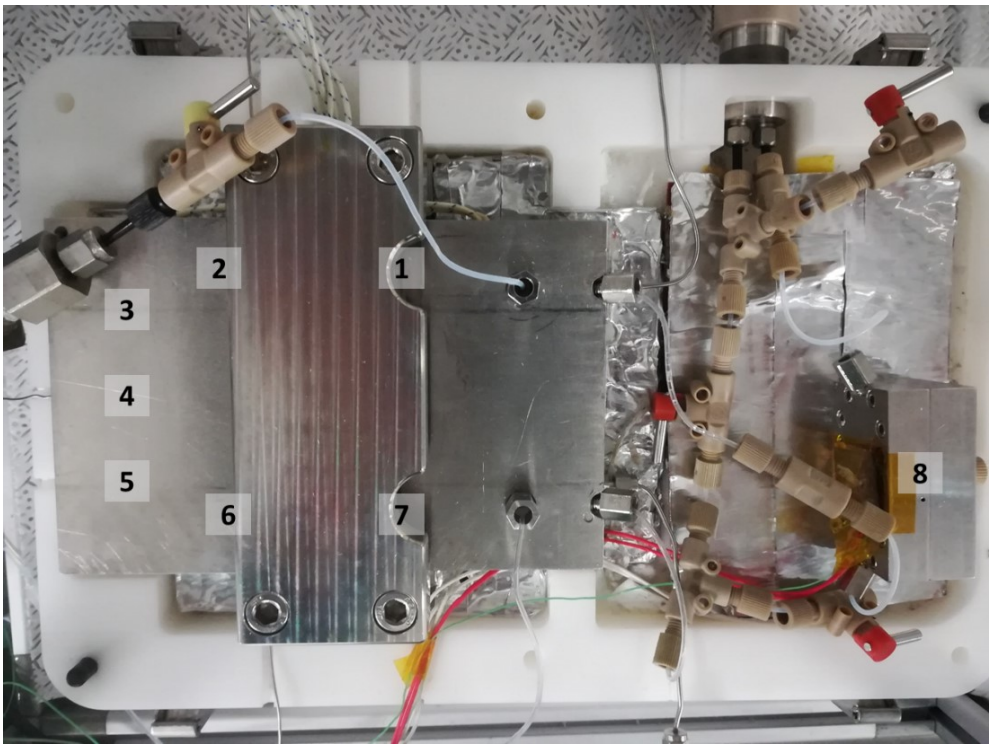

Figure S13. Picture of the slurry loop membrane reactor without insulating sheets. Numbers indicate where thermocouples were inserted for temperature measurements in the saturator (left) and the filter (right).

Table S2.

Temperature measurements in the saturator and the filter during the continuous solvent-free aerobic oxidation of benzyl alcohol using 1 wt% Au-Pd/TiO_2 powder catalyst, at a temperature setpoint of 110 °C. Refer to Table 3 for the reaction conditions and to Figure S13 for the thermocouple position.

Component	Thermocouple position	Temperature, °C
Saturator	1	111
	2	111
	3	112
	4	112
	5	108
	6	109
	7	109
Filter	8	110

Continuous operation

The substrate conversion and product selectivity results from the continuous aerobic oxidation of benzyl alcohol, cinnamyl alcohol, geraniol, 1-phenylethanol and piperonyl alcohol are reported below.

Benzyl alcohol

The solvent-free oxidation of benzyl alcohol was performed for 7 h (see Figure S14). No noticeable decrease in conversion was observed in the last 4 h of operation. In the case of the oxidation of diluted benzyl alcohol (Figure S15) conversion was higher (74%) with a 82% selectivity to benzaldehyde and only 2% to toluene. In both cases steady-state was reached after approximately 1 h, corresponding to 4 times the mean residence time of 14 min.

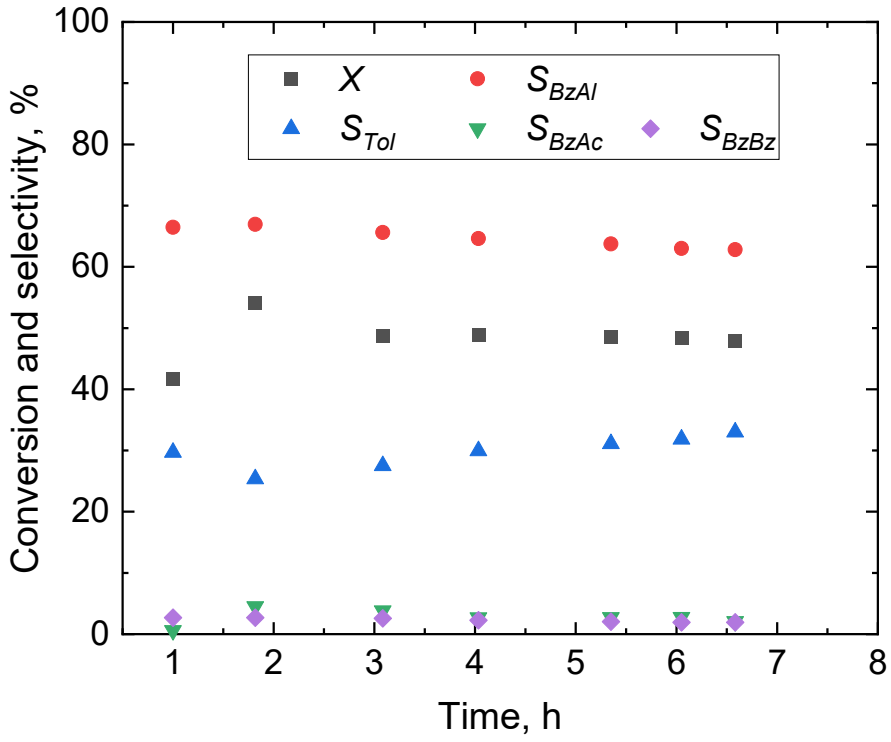

Figure S14. Benzyl alcohol conversion, X, benzaldehyde, S_{BzAl}, toluene selectivity, S_{Tol}, benzoic acid selectivity, S_{BzAc}, and benzyl benzoate selectivity, S_{BzBz}, during 7 h of solvent-free continuous aerobic oxidation of benzyl alcohol using 1 wt% Au-Pd/TiO_2 powder catalyst. Internal standard inlet concentration: 0.05 M mesitylene, inlet flowrate: 100 µL/min, recycle flowrate: 10 mL/min, oxygen pressure: 6 bar, temperature: 110 °C, catalyst concentration: 10 g/L, reactor volume: 1.4 cm^3, membrane specific surface area: 34.6 cm^{-1}.

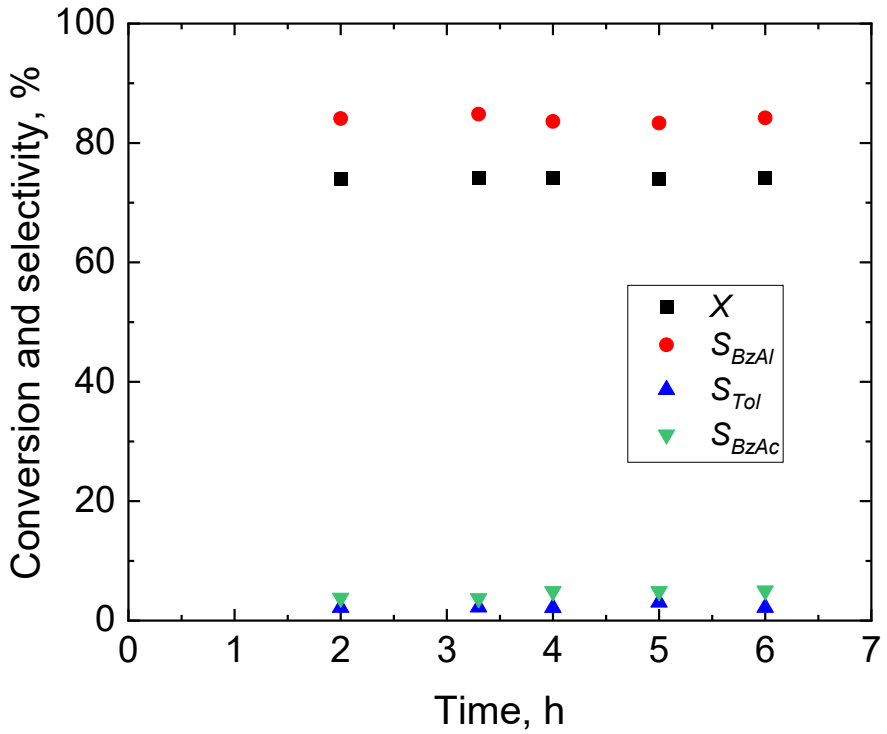

Figure S15. Benzyl alcohol conversion, *X*, benzaldehyde, S_{BzAl}, toluene selectivity, S_{Tol} and benzoic acid selectivity, S_{BzAc}, during 6 h of continuous aerobic oxidation of benzyl alcohol using 1 wt% Au-Pd/TiO_2 powder catalyst. Benzyl alcohol inlet concentration: 0.1 M, internal standard inlet concentration: 0.05 M mesitylene, solvent: *tert*-butylbenzene, inlet flowrate: 100 µL/min, recycle flowrate: 10 mL/min, oxygen pressure: 5 bar, temperature: 120 °C, catalyst concentration: 10 g/L, reactor volume: 1.4 cm^3, membrane specific surface area: 34.6 cm^{-1}.

Conversion and product selectivity from the solvent-free benzyl alcohol oxidation performed in a 8.8 cm^3 reactor (scaled-up) are reported in Figure S16. Steady-state was reached in *ca.* 2.5 h, given a mean residence time of 40 min. Conversion stabilised at 35% in the last 2 h, while benzaldehyde selectivity was around 60%. Selectivity to the main by-products (benzoic acid and benzyl benzoate) was lower than 5%. The scaled-up oxidation of benzyl alcohol was also performed in *tert*-butylbenzene and Figure S17 shows the results. Steady-state was achieved in *ca.* 1.5 h, given a mean residence time of 24 min. Benzyl alcohol conversion was 84%, 86% of which was converted to benzaldehyde, while toluene selectivity was around 1%. The main

by-products were benzoic acid, whose selectivity was around 5% and benzene with a selectivity of 6%.

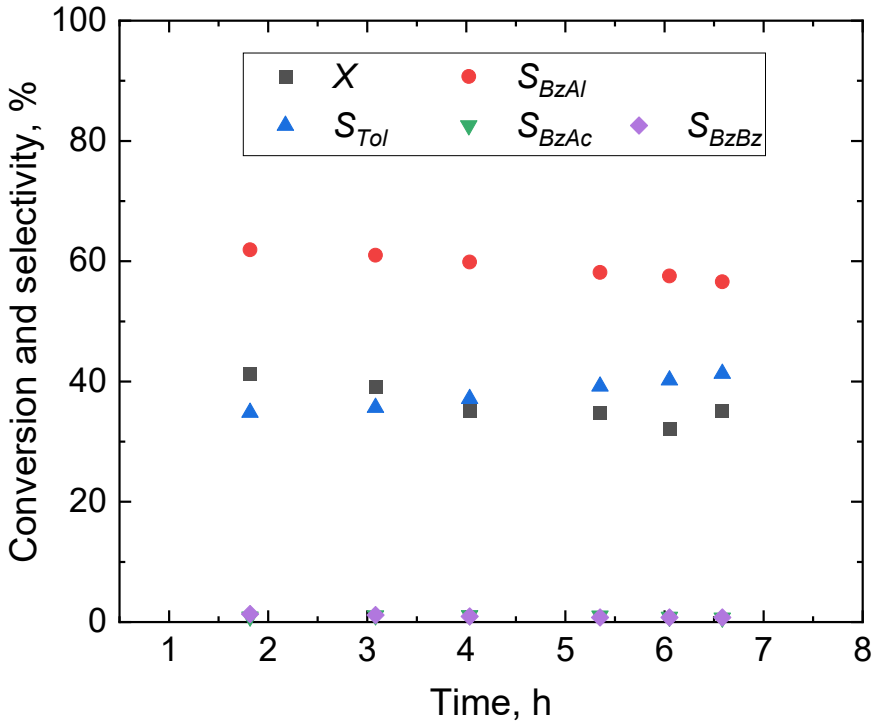

Figure S16. Benzyl alcohol conversion, X, benzaldehyde, S_{BzAl}, toluene selectivity, S_{Tol}, benzoic acid selectivity, S_{BzAc}, and benzyl benzoate selectivity, S_{BzBz}, during 7 h of solvent-free scaled-up continuous aerobic oxidation of benzyl alcohol using 1 wt% Au-Pd/TiO_2 powder catalyst. Internal standard inlet concentration: 0.05 M mesitylene, inlet flowrate: 220 µL/min, recycle flowrate: 36 mL/min, oxygen pressure: 5 bar, temperature: 120 °C, catalyst concentration: 10 g/L, reactor volume: 8.8 cm^3, membrane specific surface area: 5.5 cm^{-1}.

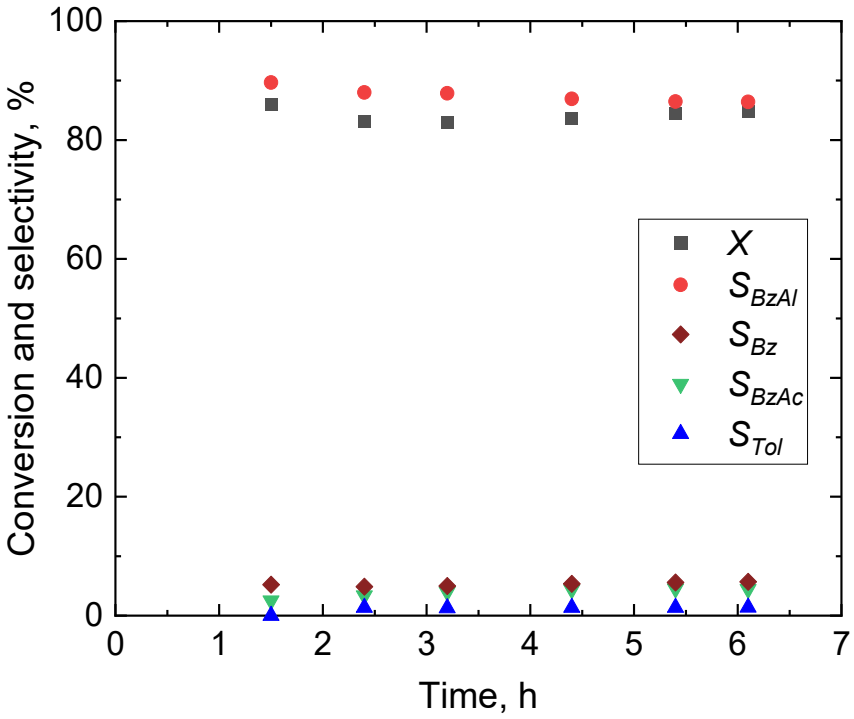

Figure S17. Benzyl alcohol conversion, X, benzaldehyde, S_{BzAl}, toluene selectivity, S_{Tol}, benzoic acid selectivity, S_{BzAc}, and benzyl benzoate selectivity, S_{BzBz}, during 6 h of scaled-up continuous aerobic oxidation of benzyl alcohol using 1 wt% Au-Pd/TiO_2 powder catalyst. Benzyl alcohol inlet concentration: 0.1 M, internal standard inlet concentration: 0.05 M mesitylene, inlet flowrate: 360 µL/min, recycle flowrate: 36 mL/min, oxygen pressure: 5 bar, temperature: 120 °C, catalyst concentration: 10 g/L, reactor volume: 8.8 cm^3, membrane specific surface area: 5.5 cm^{-1}.

Cinnamyl alcohol

Diluted cinnamyl alcohol was oxidised at 100 °C and 2 bar oxygen pressure, and its conversion and selectivity to cinnamaldehyde and 3-phenyl-1-propanol are reported in Figure S18. Results from the scaled-up reaction, performed in a 8.8 cm^3 reactor (88 mg catalyst), are shown in Figure S19. Steady-state was reached after almost 1 h in the first case, and 3 h for the scaled-up reaction (four times the mean residence time).

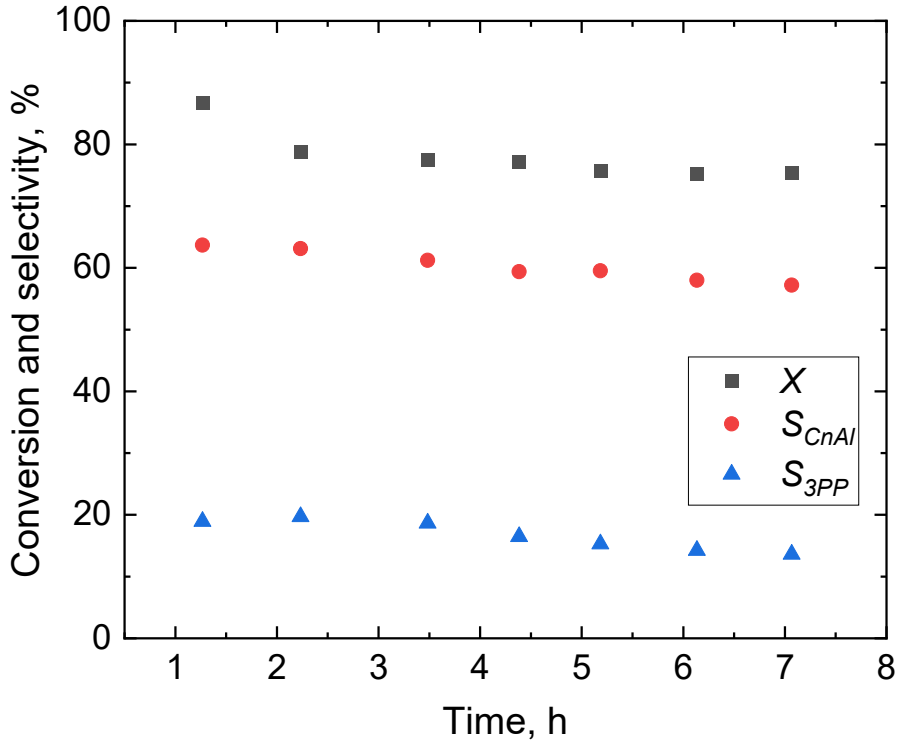

Figure S18. Cinnamyl alcohol conversion, X, cinnamaldehyde, S_{CnAl}, and 3-phenyl-1-propanol selectivity, S_{3PP}, during 7 h of continuous aerobic oxidation of cinnamyl alcohol using 1 wt% Au-Pd/TiO_2 powder catalyst. Cinnamyl alcohol inlet concentration: 0.1 M, internal standard inlet concentration: 0.05 M, inlet flowrate: 100 µL/min, recycle flowrate: 10 mL/min, oxygen pressure: 2 bar, temperature: 100 °C, catalyst concentration: 10 g/L, reactor volume: 1.4 cm^3, membrane specific surface area: 34.6 cm^{-1}.

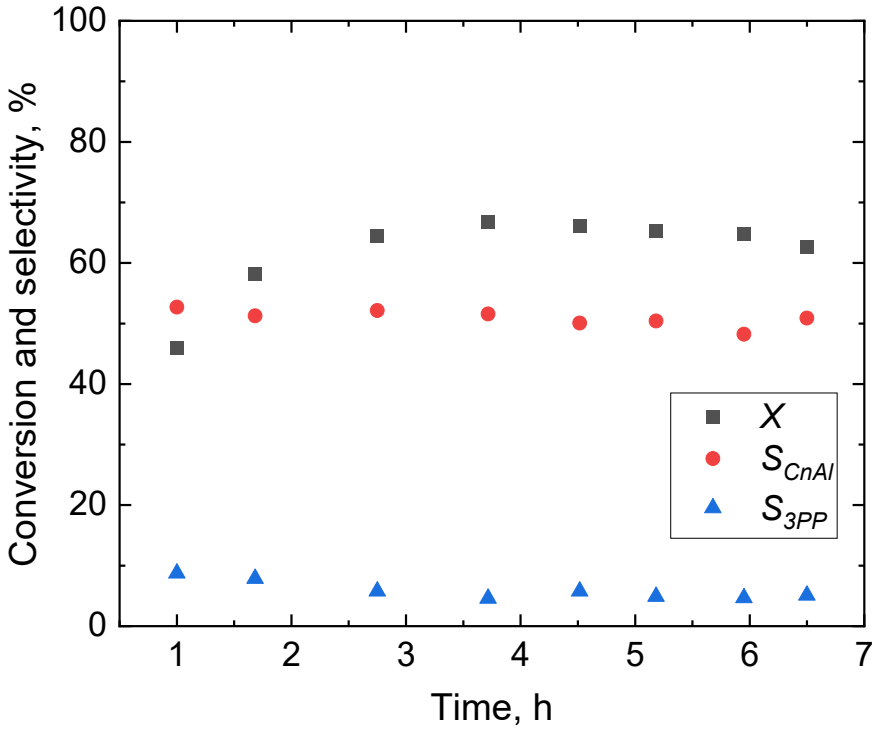

Figure S19. Cinnamyl alcohol conversion, *X*, cinnamaldehyde, S_{CnAl}, and 3-phenyl-1-propanol selectivity, S_{3PP}, during 7 h of scaled-up continuous aerobic oxidation of cinnamyl alcohol using 1 wt% Au-Pd/TiO_2 powder catalyst. Cinnamyl alcohol inlet concentration: 0.1 M, internal standard inlet concentration: 0.05 M, inlet flowrate: 200 µL/min, recycle flowrate: 36 mL/min, oxygen pressure: 2 bar, temperature: 100 °C, catalyst concentration: 10 g/L, reactor volume: 8.8 cm^3, membrane specific surface area: 5.5 cm^{-1}.

Geraniol

Geraniol was oxidised and its conversion and selectivity to geranial are reported in Figure S20. Due to the lower inlet flowrate (20 µL/min), steady-state was reached after 4 h from the start-up, given a mean residence time of 70 min. Selectivity to geranial was found to be higher at low conversion and lower (*ca.* 28%) when conversion increased to around 28%.

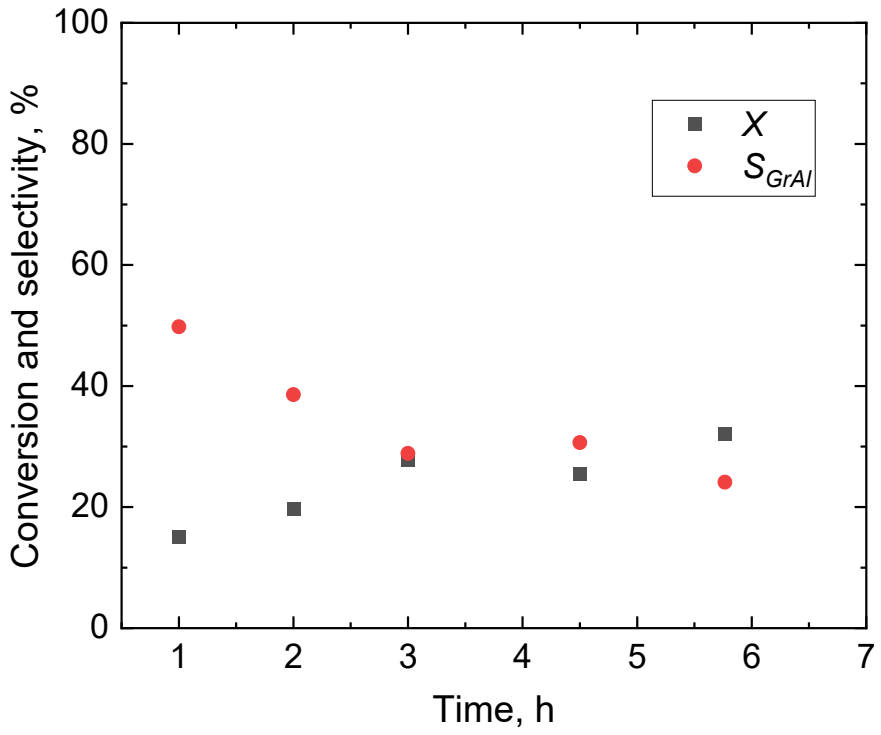

Figure S20. Geraniol conversion, *X*, and geranial selectivity, S_{GrAl}, during 6 h of continuous aerobic oxidation of geraniol using 1 wt% Au-Pd/TiO_2 powder catalyst. Geraniol concentration: 0.1 M, internal standard inlet concentration: 0.05 M, inlet flowrate: 20 µL/min, recycle flowrate: 10 mL/min, oxygen pressure: 6 bar, temperature: 120 °C, catalyst concentration: 10 g/L, reactor volume: 1.4 cm^3, membrane specific surface area: 34.6 cm^{-1}.

1-Phenylethanol

Conversion of 1-phenylethanol and its selectivity to acetophenone are reported in Figure S21. Conversion stabilised to *ca.* 30% with 100% selectivity to acetophenone. Steady-state was achieved after 1.2 h, given a mean residence time of 18 min.

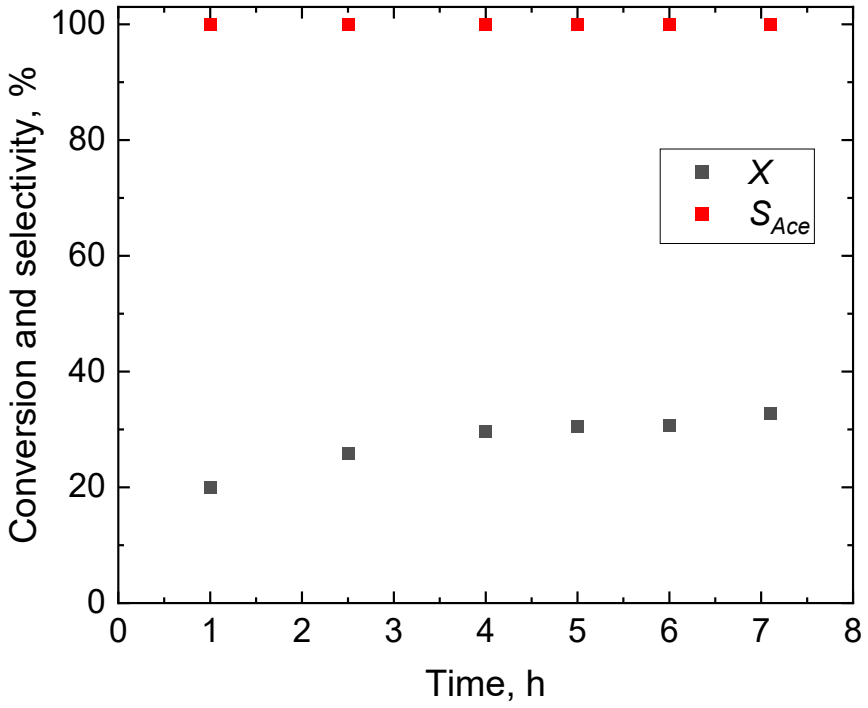

Figure S21. 1-Phenylethanol conversion, *X*, and acetophenone selectivity, S_{Ace}, during 7 h of continuous aerobic oxidation of 1-phenylethanol using 1 wt% Au-Pd/TiO_2 powder catalyst. 1-Phenylethanol concentration: 0.1 M, internal standard inlet concentration: 0.05 M, inlet flowrate: 80 µL/min, recycle flowrate: 10 mL/min, oxygen pressure: 6 bar, temperature: 120 °C, catalyst concentration: 10 g/L, reactor volume: 1.4 cm^3, membrane specific surface area: 34.6 cm^{-1}.

Piperonyl alcohol

The oxidation products of piperonyl alcohol were analysed by manually injecting the reaction samples in a GC-MS (QP2010 SE, Shimadzu). A typical spectrum is shown in Figure S22. At retention times of 7.7 min and 8 min, mesitylene, the internal standard, and the solvent, *tert*-butylbenzene, are observed. Piperonal was separated after 12 min and this was the only detected product, while piperonyl alcohol eluted after 12.3 min.

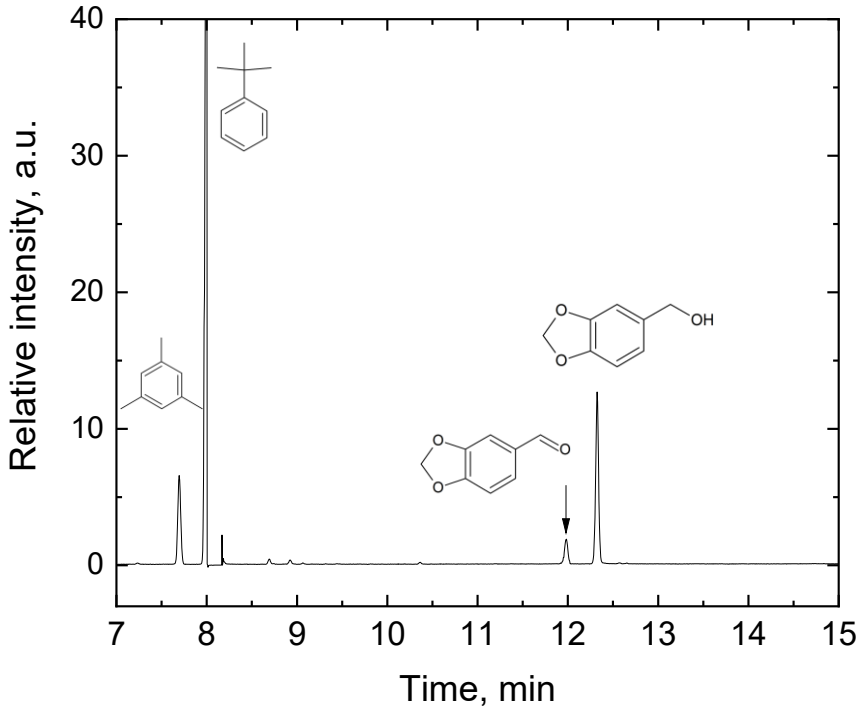

Figure S22. GC-MS spectrum for the piperonyl alcohol continuous aerobic oxidation products.

Piperonal concentration was estimated by dividing the area under its peak with that of piperonyl alcohol, multiplied by the known piperonyl alcohol concentration. This was done assuming similar relative response factors between the two molecules. The response factor of a flame ionisation detector is mainly a function of the carbon number and the molecular weight of a molecule and its value does not differ much between molecules with a hydroxyl group and a corresponding carbonyl group [3].

Figure S23 shows the piperonyl alcohol conversion and piperonal selectivity over 6.5 h continuous reaction. Steady state was achieved after 3 h, corresponding to 4 times the mean residence time of 47 min.

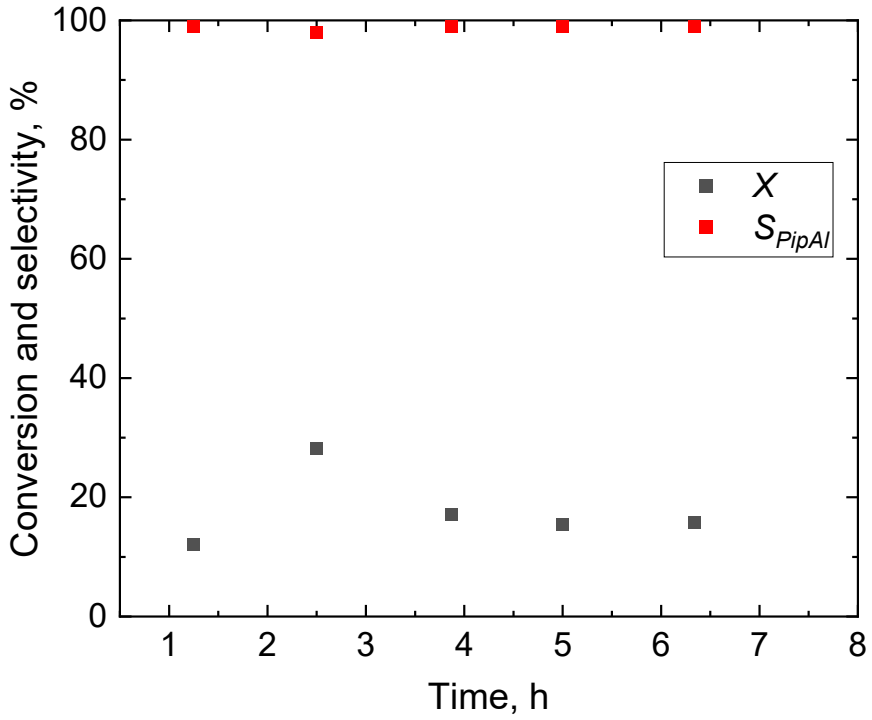

Figure S23. Piperonyl alcohol conversion, X, and piperonal selectivity, S_{PipAl}, during 6.5 h of continuous aerobic oxidation of piperonyl alcohol using 1 wt% Au-Pd/TiO_2 powder catalyst. Piperonyl alcohol inlet concentration: 0.1 M, internal standard inlet concentration: 0.05 M, inlet flowrate: 30 µL/min, recycle flowrate: 10 mL/min, oxygen pressure: 5 bar, temperature: 120 °C, catalyst concentration: 10 g/L, reactor volume: 1.4 cm^3, membrane specific surface area: 34.6 cm^{-1}.

Unlike in the continuous reaction, the batch oxidation of piperonyl alcohol produced other products (Figure S24). These include 1,3-benzodioxole (8.5 min), 3,4-methylenedioxy toluene (12.6 min) and piperonylic acid (14 min), the latter possibly resulting from the oxidation of piperonal. Piperonal concentration was estimated as described above and a selectivity of 65% was determined.

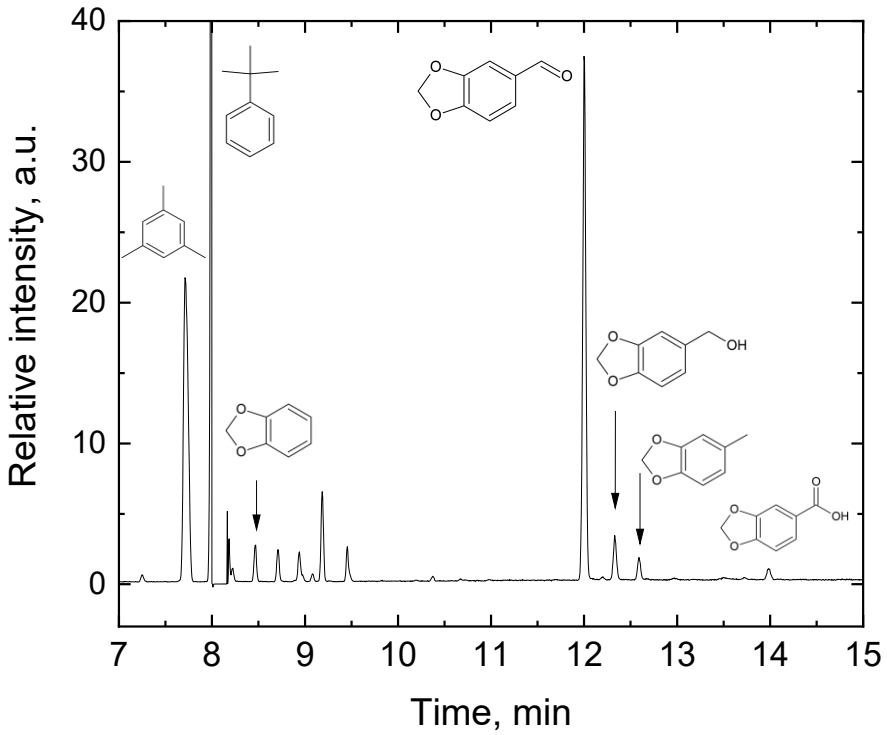

Figure S24. GC-MS spectrum for the piperonyl alcohol batch aerobic oxidation products.

Pervaporation rate and safety considerations

In the scaled-up continuous oxidation experiments, pure oxygen was fed to the gas channel at a flowrate of 30 NmL/min (measured under normal conditions: 20 °C and 1 atm). A cold trap (0 °C, 1 atm) installed at the gas outlet ensured the condensation of the organic vapours entrained in the flowing gas. The condensed liquid was collected in a vial and the amount weighed at the end of the experiment. For reactions conducted in *tert*-butylbenzene, no organic vapour condensed in the vial. This could be ascribed to the high boiling point of the solvent (169 °C) and to the low concentration of the alcohol substrates in the reaction. However, in the scaled-up continuous solvent-free oxidation of benzyl alcohol an amount of 0.341 g of organics was collected after 6 h reaction and analysed at the GC. Equation (S19) was used to calculate the outlet mass flowrate for each component in the gas phase, $\dot{m}_i$, where MM_i is the corresponding molar mass, $\dot{m}_{vap}$ the average overall mass flowrate of organics in the gas phase during 6 h of operation (57 mg/h) and c_i is the molar concentration of each component in the collected liquid. The molar concentration of each component in the gas phase, y_i, was derived using Equation (S20), where v_{O2} is the oxygen flowrate (30 NmL/min), R_g the ideal gas constant (8.3145 J/mol/K), T the absolute temperature (393 K) and p_{O2} the oxygen pressure (5 bar).

$$\dot{m}_i = \frac{c_i\, MM_i}{\sum_i c_i\, MM_i} \dot{m}_{vap} \tag{S19}$$

$$y_i = \frac{\dot{m}_i}{MM_i} \frac{R_g T}{p_{O_2}\, v_{O_2}} \tag{S20}$$

The sum of the molar fractions of benzyl alcohol, benzaldehyde and toluene in the gas phase was 0.20%. The lower flammability limit for each component in pure oxygen, $LFL_{oxy,i}$, can be estimated using the approach developed by Chen [4]. Equation (S21) can be applied to benzaldehyde and benzyl alcohol, as the *LFL* of toluene in oxygen is reported to be 1.01% [5]. In the equation, $LFL_{air,i}$ is the lower flammability limit in air of the i-th component, while $\hat{c}_{p,O2}$ and $\hat{c}_{p,N2}$ are the molar heat capacities of oxygen (30 J/mol/K, [6]) and nitrogen (31 J/mol/K, [4]), respectively.

$$LFL_{oxy,i} = \frac{LFL_{air,i}\, \hat{c}_{p,O_2}}{LFL_{air,i}\, \hat{c}_{p,O_2} + \left(1 - LFL_{air,i}\right)\left(0.21\, \hat{c}_{p,O_2} + 0.79\, \hat{c}_{p,N_2}\right)} \tag{S21}$$

Benzyl alcohol has a LFL_{air} of 1.3%, similar to that of benzaldehyde, 1.4% [7, 8]. Applying Chen's method, the lower flammability limits in oxygen of benzyl alcohol and benzaldehyde are estimated to be equal to 1.25% and 1.35%, respectively, and still above toluene's *LFL* in oxygen. It is important to highlight that these flammability limits refer to atmospheric pressure. However, the dependence of the *LFL* on pressure is small and it can be assumed negligible for the operating conditions described in this work [9].

To calculate the lower flammability limit of a mixture of components, LFL_{mix}, LeChatelier's mixing rule, shown in Equation (S22), was used, where n is the number of components with a specific molar fraction on a combustible basis, x_i [10].

$$LFL_{mix} = \left(\sum_i^n \frac{x_i}{LFL_i} \right)^{-1} \quad \text{(S22)}$$

Given the individual $LFL_{oxy,i}$, the lower flammability limit of the organics mixture in oxygen was estimated to be 1.23 mol%. Therefore, we can conclude that the concentration of organics (0.20 mol%) was outside the flammability window and hence the continuous scaled-up aerobic oxidation of benzyl alcohol was operated under safe conditions.

References

[1] I. K. Stamatiou and F. L. Muller, *AIChE J.*, 2017, **63**, 273-282.

[2] I. Pinnau and L. G. Toy, *J. Memb. Sci.*, 1996, **109**, 125-133.

[3] A. D. Jorgensen, K. C. Picel and V. C. Stamoudis, *Anal. Chem.*, 1990, **62**, 683-689.

[4] C.-C. Chen, *Ind. Eng. Chem. Res.*, 2011, **50**, 10283-10291.

[5] D. Kong, D. J. am Ende, S. J. Brenek and N. P. Weston, *J. Hazard. Mater.*, 2003, **102**, 155-165.

[6] D. Tromans, *Hydrometallurgy*, 1998, **48**, 327-342.

[7] F. Brühne and E. Wright, in *Ullmann's Encyclopedia of Industrial Chemistry*, Wiley-VCH, Weinheim, 2012, vol. 5, pp. 357-366.

[8] F. Brühne and E. Wright, in *Ullmann's Encyclopedia of Industrial Chemistry*, Wiley-VCH, Weinheim, 2012, vol. 5, pp. 223-236.

[9] M. G. Zabetakis, *AIChE Symp. Ser.*, 1965, **2**, 99-104.

[10] C. V. Mashuga and D. A. Crowl, *Process Saf. Prog.*, 2000, **19**, 112-117.